

Glutathione depleting pro-oxidant as a selective anticancer therapeutic agent

Donghyuck Yoo¹, Eunkyeong Jung¹, Joungyoun Noh², Hyejin Hyun¹, Semee Seon¹, Seri Hong¹, Dongin Kim³, Dongwon Lee^{1,2,}*

¹Department of BIN Convergence Technology and ²Department of Polymer-Nano Science and Technology, Chonbuk National University, Backjedaero 567, Jeonju, Chonbuk, 54896, Republic of Korea

³Department of Pharmaceutical Sciences, Texas A&M University, College Station, Texas, 77843, United States

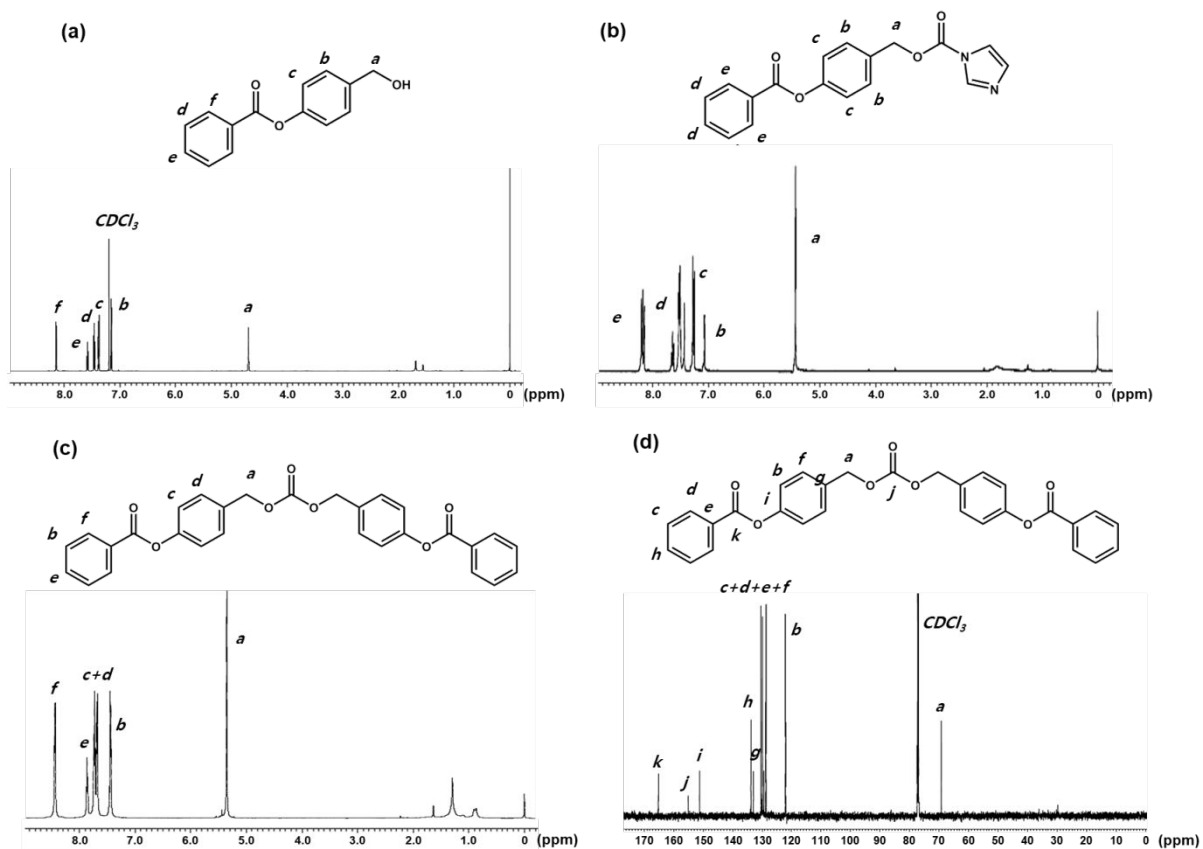


Figure S1. Characterization of compounds compound 1, 2 and 3. (a) ^1H NMR spectrum of compound 1. (b) ^1H NMR spectrum of compound 2. (c) ^1H NMR spectrum of compound 3. (d) ^{13}C NMR spectrum of compound 3.

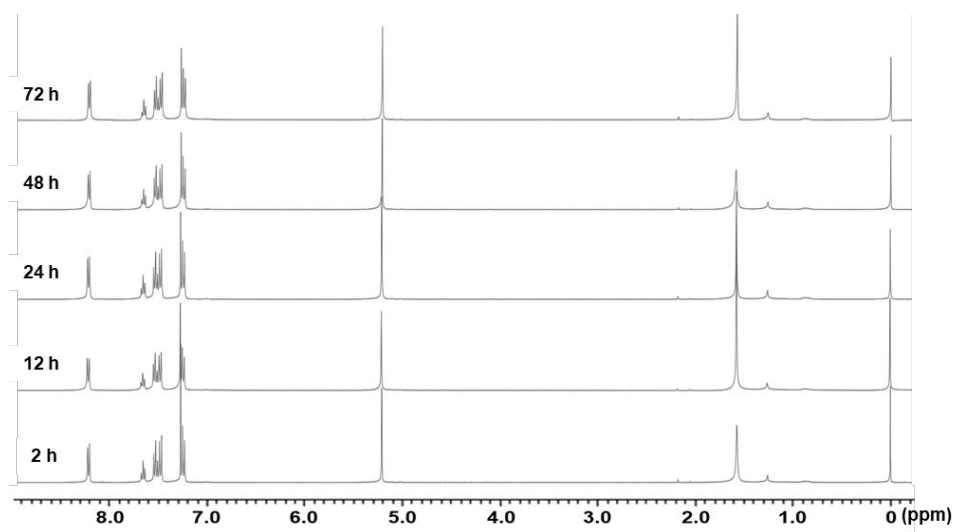


Figure S2. NMR spectra of B2C after incubation under aqueous conditions.

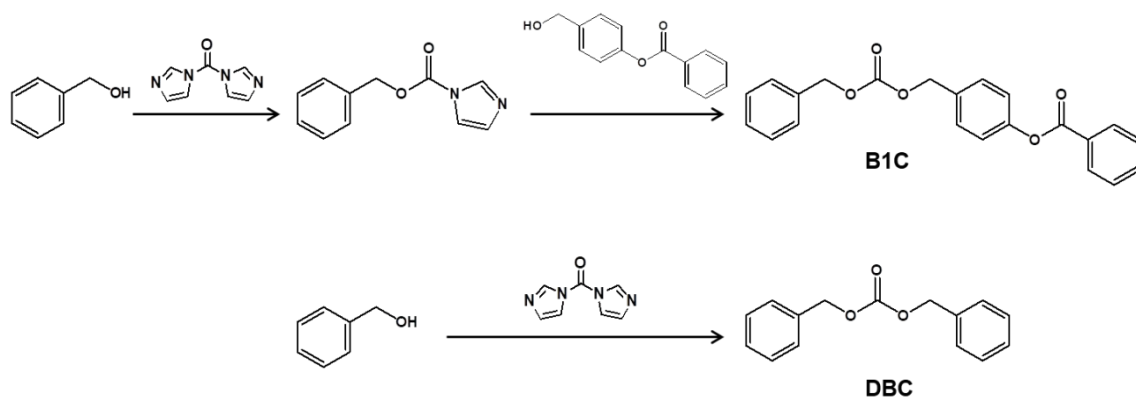


Figure S3. Synthetic routes of B1C and DBC.

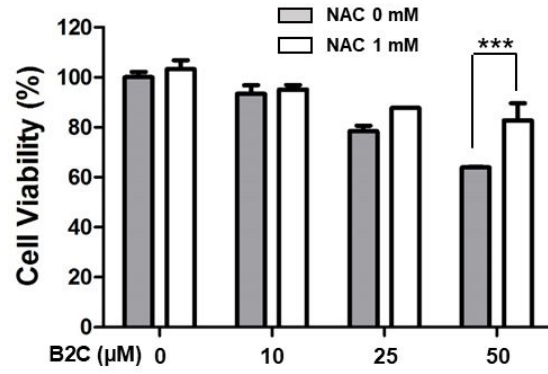


Figure S4. Cytotoxicity of B2C against RAW264.7 cells in the presence or absence of NAC. *** $p < 0.001$. Values are mean \pm S.D (n=4).

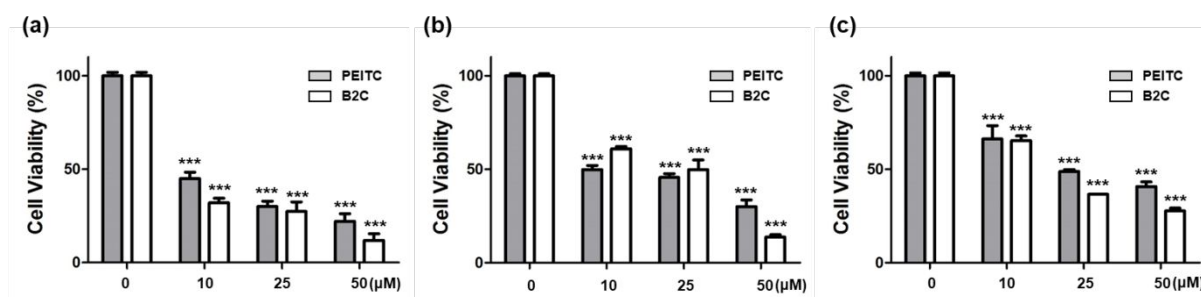


Figure S5. Comparison of cytotoxicity between B2C and PEITC. Values are mean±S.D (n=4). **<0.01, ***p<0.001 relative to 0 μM B2C. †††p<0.001 relative to the same concentration of PEITC.

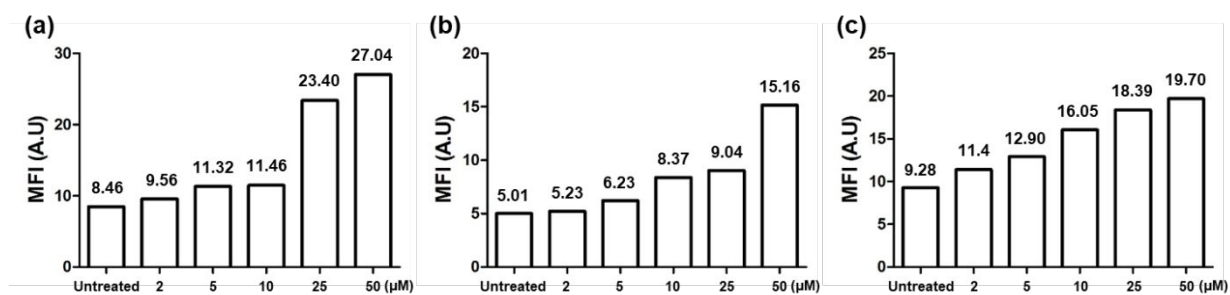


Figure S6. Quantification of intracellular ROS in B2C-treated cells. (a) SW620 cells. (b) DU145 cells. (c) A549 cells.

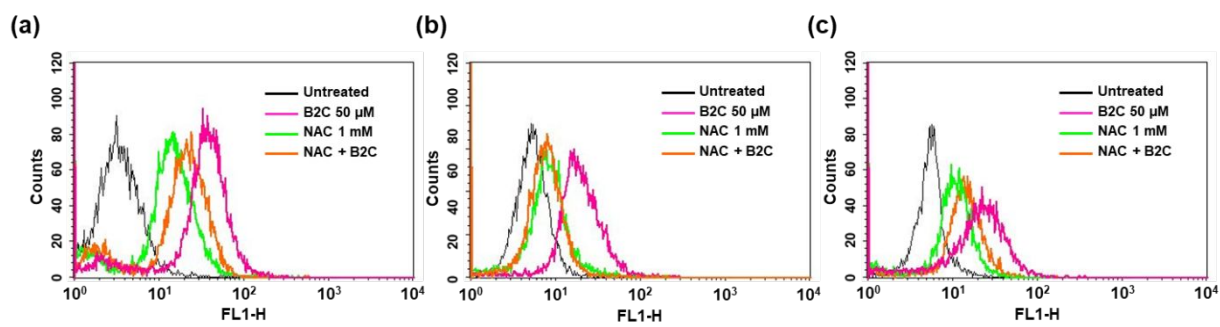


Figure S7. The level of intracellular ROS in B2C-treated cells in the presence of NAC. (a) SW620 cells. (b) DU145 cells. (c) A549 cells.

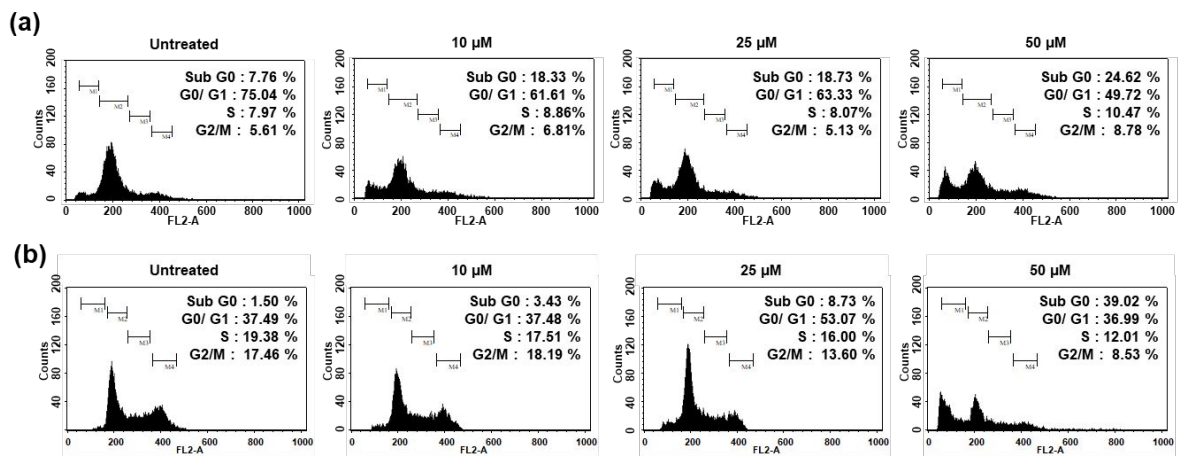


Figure S8. Cell cycle assay of cancer cells after the treatment with B2C. (a) DU145 cells. (b) A549 cells.

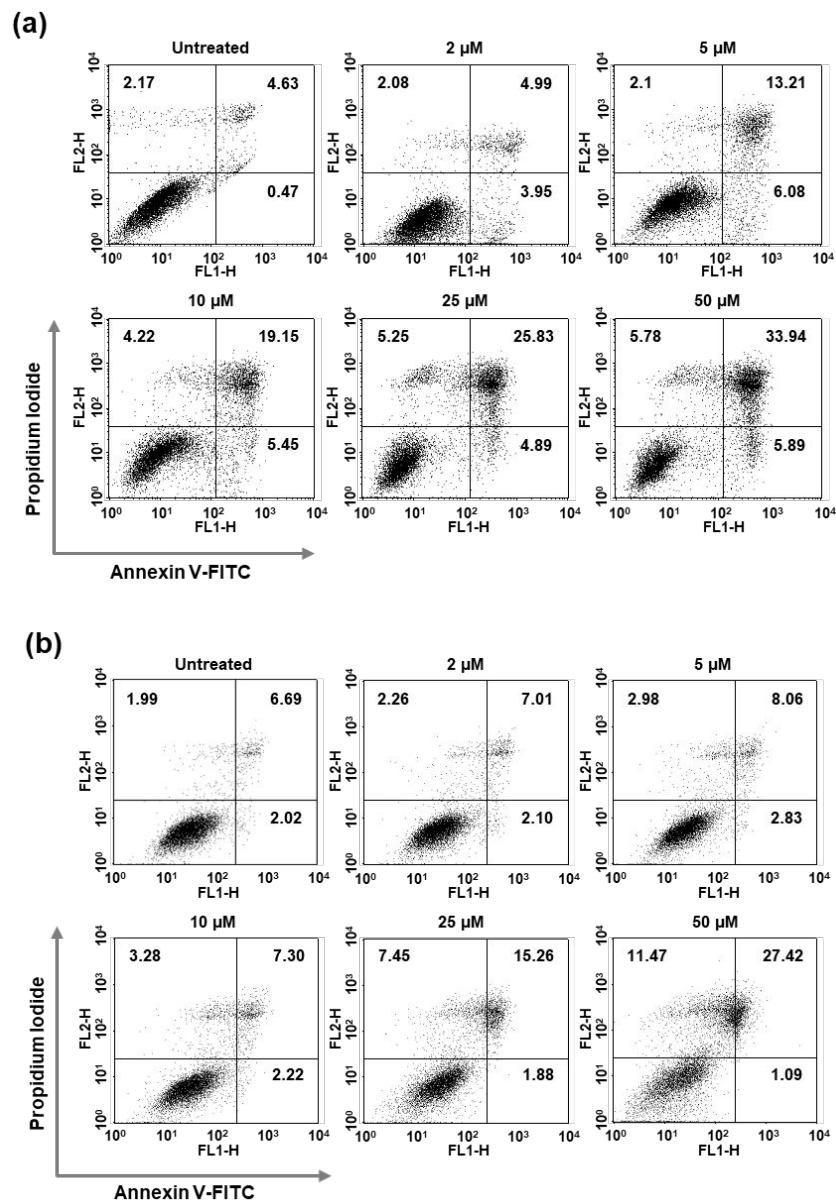


Figure S9. Flow cytometric analysis of apoptotic cell death using Annexin V-FITC and propidium iodide. (a) DU145 cells. (b) A549 cells.

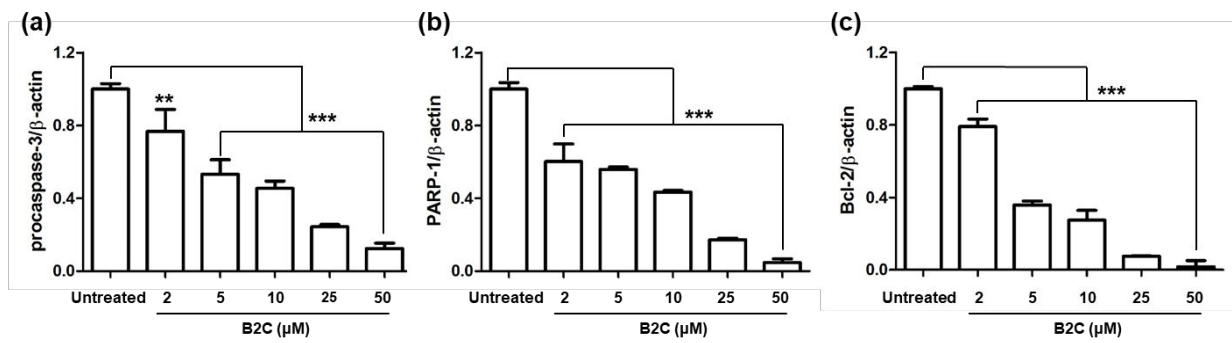


Figure S10. Quantification of apoptosis-related proteins. (a) Procaspase-3. (b) PARP-1. (c) Bcl-2. $**p < 0.01$, $***p < 0.001$. Values are mean \pm S.D (n=4).

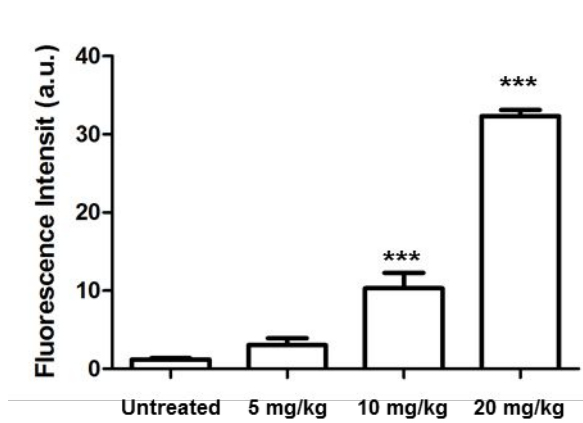


Figure S11. Quantification of apoptotic cell death in tumors. Values are mean \pm S.D (n=4).
***p<0.001 relative to Untreated.

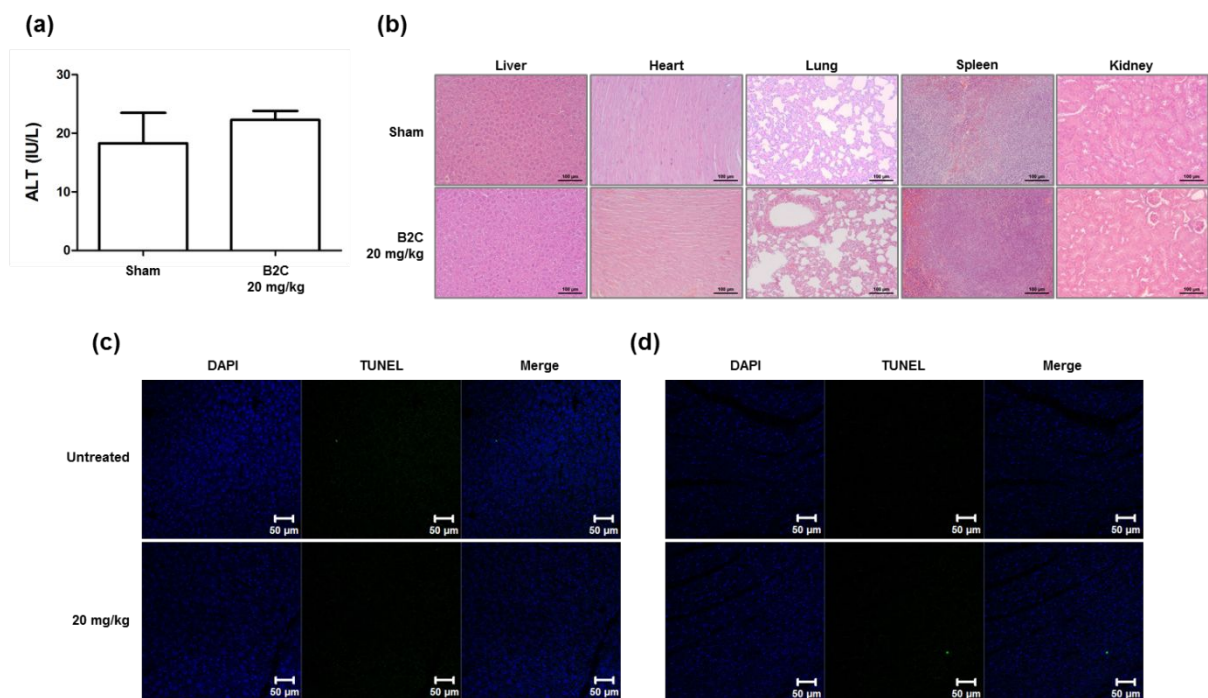


Figure S12. *In vivo* toxicity studies of B2C using normal mice. (a) The level of ALT. (b) Representative H&E staining images of organ tissues. TUNEL stained images of liver (c) and heart (d). Values are mean \pm S.D (n=4).

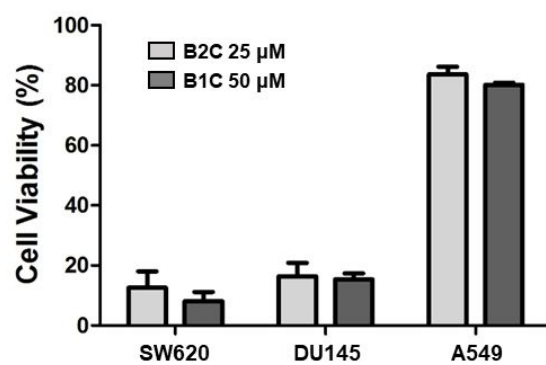


Figure S13. Comparison of cytotoxicity of 25μM of B2C with 50μM B1C. Data are from Figure 3.

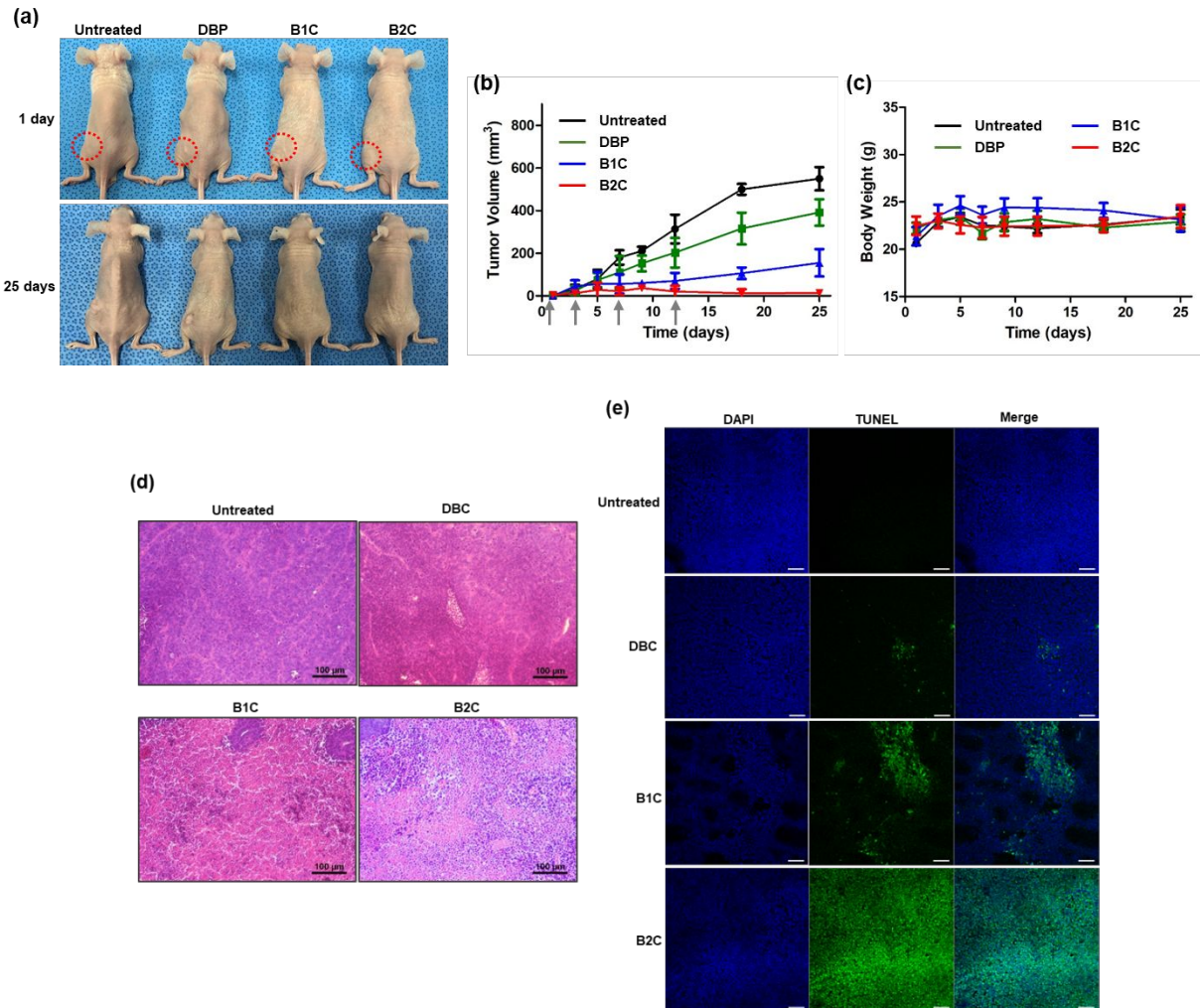


Figure S14. Comparison of therapeutic efficacy between B2C and B1C. (a) Photographs of tumor-bearing mice treated with B2C, B1C or DBP. Red dotted lines indicate inoculation sites of SW620 cells. (b) Changes in tumor volumes during the treatment. Arrows indicate the date of injection. (c) Body weight changes of tumor-bearing mice during the treatment. Values are mean±S.D (n=4). (d) Micrographs of tumor sections stained with H&E. (e) Micrographs of tumor sections stained with TUNEL.

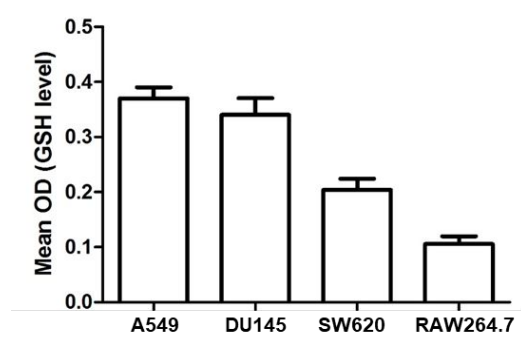


Figure S15. The level of GSH in various cells. Values are mean \pm S.D (n=4).